



Synthesis of Pd and Nb–doped TiO₂ composite supports and their corresponding Pt–Pd alloy catalysts by a two-step procedure for the oxygen reduction reaction

Yan-Jie Wang^{a,b}, David P. Wilkinson^{a,b,*}, Alan Guest^a, Vladimir Neburchilov^a, Ryan Baker^a, Feihong Nan^c, Gianluigi A. Botton^c, Jiu-Jun Zhang^{a,**}

^a Institute for Fuel Cell Innovation, National Research Council Canada (NRC-IFCI), Vancouver, BC Canada V6T 1W5

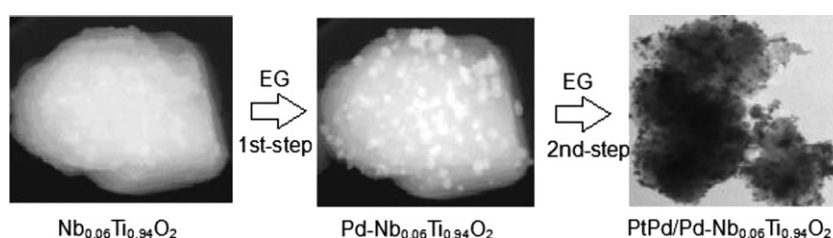
^b Department of Chemical and Biological Engineering (UBC), University of British Columbia, Vancouver, BC Canada V6T 1Z3

^c Department of Materials Science and Engineering, McMaster University, 1280 Main Street West, Hamilton, Ontario L8S 4L7, Canada

HIGHLIGHTS

- Highly conductive Pd–Nb_{0.06}Ti_{0.94}O₂ supports were obtained with the addition of Pd.
- The supported Pt–Pd catalysts were prepared by a polyol deposition method.
- The conductivity of support increased with increasing content of Pd.
- Pt–Pd nanoparticles adhered to Pd–Nb_{0.06}Ti_{0.94}O₂ surfaces to form Pt_mPd_n clusters.
- Pt_mPd_n facilitate the dissociation of O₂ on the Pt surface and enhance ORR activity.

GRAPHICAL ABSTRACT



ARTICLE INFO

Article history:

Received 30 June 2012

Received in revised form

7 August 2012

Accepted 9 August 2012

Available online 18 August 2012

Keywords:

PEM fuel cells

Oxygen reduction reaction

Conductivity

Mass activity

Clusters

Composite support

ABSTRACT

Several Pd–composite Nb_{0.06}Ti_{0.94}O₂ materials are synthesized by a two-step procedure, and employed as the Pt–Pd alloy catalyst support for the PEM fuel cell oxygen reduction reaction (ORR). These supports and their supported catalysts are characterized using analytical and electrochemical methods with respect to their material morphology, chemical/electrochemical stability, electronic conductivity as well as oxygen reduction reaction (ORR) mass activity/stability. For the supported Pt–Pd catalysts, the Pt–Pd nanoparticles adhered to both the Nb_{0.06}Ti_{0.94}O₂ and composited Pd surfaces to form Pt_mPd_n clusters. A possible synergetic interaction between the Pt–Pd alloy catalyst and its Pd–Nb_{0.06}Ti_{0.94}O₂ composite support is believed to exist which enhances the ORR activity of these catalysts. The electronic conductivity of Nb_{0.06}Ti_{0.94}O₂ can be greatly improved after forming composites with Pd to the desired levels required for electrocatalyst applications. Three supported Pt–Pd catalysts, 20 wt% Pt_{0.62}Pd_{0.38}/Pd₁₀wt%–(Nb_{0.06}Ti_{0.94}O₂)₉₀wt%, 20 wt% Pt_{0.62}Pd_{0.38}/Pd₃₀wt%–(Nb_{0.06}Ti_{0.94}O₂)₇₀wt%, and 20 wt% Pt_{0.62}Pd_{0.38}/Pd₅₀wt%–(Nb_{0.06}Ti_{0.94}O₂)₅₀wt%, are synthesized and tested using both cyclic voltammetric and rotating disk electrode techniques with respect to their surface electrochemistry, ORR mass activity, and electrochemical stability. All three catalysts show higher Pt mass activity (>130 mA mg_{Pt}^{−1} at 0.9 V vs. RHE) than that of the baseline 47 wt% Pt C^{−1} carbon supported catalyst (110 mA mg_{Pt}^{−1}). However, the durability of these catalysts needs to be further improved.

© 2012 Published by Elsevier B.V. All rights reserved.

* Corresponding author. Department of Chemical and Biological Engineering (UBC), University of British Columbia, Vancouver, BC Canada V6T 1Z3. Tel.: +1 604 822 4888.

** Corresponding author. Institute for Fuel Cell Innovation, National Research Council Canada, 4250 Westbrook Mall, Vancouver, BC, Canada V6T 1W5. Tel.: +1 604 221 3087.

E-mail addresses: dwilkinson@chbe.ubc.ca (D.P. Wilkinson), Jiu-Jun.Zhang@nrc.gc.ca (J. Zhang).

1. Introduction

Proton exchange membrane (PEM) fuel cells are electrochemical devices that convert the chemical energy of a fuel such as hydrogen into electricity with high efficiency. They have many advantages such as high energy density, high power density, and low/zero emissions which have made them very promising in several important applications such as transportation, stationary and portable power [1–4]. PEM fuel cells are approaching full commercialization, but two major challenges, high cost and insufficient durability, have been recognized as barriers toward further progress [5–9]. Both high cost and low durability are largely an issue with the Pt-based catalysts used in the PEM fuel cell for both the oxygen reduction reaction (ORR) at the cathode and the hydrogen oxidation reaction (HOR) at the anode. With the current state of technology, carbon supported Pt-based catalysts are still the most practical catalysts for fuel cell reactions [4,10–14]. Therefore, for near term commercialization, reducing the cost of Pt catalysts and increasing their stability at the same time seems to be a necessary approach.

With respect to the durability issues with PEM fuel cells, catalyst degradation caused by carbon support oxidation, Pt particle agglomeration, sintering, and dissolution have been identified as some of the major contributors. In particular, the oxidation or corrosion of the catalyst carbon support under harsh fuel cell operational conditions such as high cathode potential in the presence of oxygen and water can cause Pt particles to be separated from the carbon support, leading to isolated Pt particles. As a result, the reaction site density will be reduced, causing reduced Pt utilization and the degradation of fuel cell performance as well [15–17]. To address the corrosion issue of the carbon support, considerable effort has been put into replacing carbon using non-carbon materials [18].

In the effort to replace carbon using non-carbon materials, titanium dioxide (TiO₂)-based materials have received great attention due to their high chemical, electrochemical and thermal stability. However, both electronic conductivity and surface area have been identified as the challenges for metal oxide-based materials including TiO₂ when they are used for fuel cell catalyst supports [19,20]. Normally, the catalyst support should have a sufficient conductivity at least above 0.1 S cm^{−1} for fuel cell catalyst applications [21,22] as well as a surface area larger than 100 m² g^{−1} [23].

Although TiO₂ itself is not conductive, doping with appropriate n-type dopants like niobium (Nb) can effectively improve its conductivity because of the different valence state of Nb and the doping feasibility as a result of the similarity of the ionic radii of Nb⁵⁺ ($r = 0.70 \text{ \AA}$) and Ti⁴⁺ ($r = 0.68 \text{ \AA}$) [24–26]. Some reports [9,27] have shown that with the usage of Nb_xTi_(1-x)O₂ as a support for a Pt catalyst, the interaction between the catalyst and the support are strong enough to improve Pt specific activity for the oxygen reduction reaction (ORR). Also, the electrical conductivity of Nb-doped TiO₂ was found to strongly depend on the synthesis conditions [28]. For example, high heat-treatment temperature were found to be effective in enhancing the electrical conductivity of Nb-doped TiO₂ [9]. According to Huang et al. [9], after Nb_xTi_(1-x)O₂ ($x = 0.25$) was treated at 900 °C, its conductivity could be increased to 1.11 S cm^{−1}. However, its specific surface area was reduced from 300 to 2 m² g^{−1}, indicating that the surface area of TiO₂-based materials can be significantly decreased with increasing heat-treatment temperature. In order to obtain both high electrical conductivity and high specific surface area, some optimization is definitely required, which results in a trade-off between these parameters.

Another way to improve the electrical conductivity of the support would be to introduce conductive materials such as pure metal into the TiO₂-based material to form composite support materials. In this work, Pd, which has an electrical conductivity above 10 S cm^{−1} [29], was introduced into Nb-doped TiO₂ (Nb-TiO₂) material. After this Pd introduction, the electrical conductivity of the composite Pd and Nb-TiO₂ material showed a significant increase in conductivity from Nb-TiO₂'s 10^{−3} S cm^{−1} to 2.65 S cm^{−1}, and the resulting material also showed improved ORR electrocatalytic activity due to the interaction between the support and the PtPd catalyst. In our approach, both one-step and two-step synthesis methods were developed to synthesize composites of Pd with Nb_{0.06}Ti_{0.94}O₂ as a support material (Pd-Nb_{0.06}Ti_{0.94}O₂), and this support was used to prepare PtPd alloy catalysts (Pt_xPd_y/Pd-Nb_{0.06}Ti_{0.94}O₂). Both physical and electrochemical characterizations were carried out on these materials with respect to their structure, composition, and ORR performance, and are reported in this paper.

2. Experimental section

2.1. Chemicals

For synthesis, the following chemicals were used: titanium(IV) isopropoxide (97%, Alfa Aesar), niobium(V) ethoxide (99.999%, Alfa Aesar) and ammonium hexachloropalladate(IV) (99.9%, Alfa Aesar), hydrochloric acid (37%, Sigma–Aldrich), sodium borohydride (98%, Sigma–Aldrich), chloroplatinic acid hydrate (99.9%, Sigma–Aldrich), anhydrous ethylene glycol (99.8%, Sigma–Aldrich), and Nafion® ionomer (5 wt% in lower aliphatic alcohols and water, Sigma–Aldrich). All chemicals were used as received without further purification.

2.2. Support synthesis

In synthesizing the composite materials via a two-step procedure, the first step was to synthesize Nb-doped TiO₂ (Nb_{0.06}Ti_{0.94}O₂). A certain amount of niobium (V) ethoxide was added to 12 M hydrochloric acid with stirring for 15 min. Then, titanium(IV) isopropoxide was added to the above solution under stirring for another 15 min to form a precursor solution. This solution was then heated at 120 °C for 20 h under stirring. The produced solid was filtered out by a centrifuge, washed with deionized water, and dried in an oven at 80 °C. After that, the obtained dry solid was transferred to a furnace and reduced at 700 °C for 10 h under pure H₂ gas at a flow rate of 600 ml min^{−1}. The final product was ground in an agate mortar to obtain a fine powder of Nb_{0.06}Ti_{0.94}O₂.

In the second step to make a Pd composite support material, the Nb_{0.06}Ti_{0.94}O₂ nanoparticle powder was mixed with DI water under ultrasonication for 1.0 h to form a mixture (marked as Mixture A). For Pd precursor preparation, the calculated amount of ammonium hexachloropalladate (IV) was dissolved into a solvent containing DI water and anhydrous ethylene glycol (volume ratio of 1:5). Then this Pd⁴⁺ containing solution was placed in the center of a microwave oven (National NN-S327WF, 2450 MHz, 700 W) and heated at 250 °C for 2 min. After this heating, the resulting suspension was mixed with mixture A under stirring for 24 h, which was then filtered to obtain the solid sample. This solid sample was washed and dried at 100 °C overnight in a vacuum oven to obtain the final product. To make a fine powder, this final product was ground in an agate mortar for 0.5 h to obtain nanoparticles of Pd composited Nb_{0.06}Ti_{0.94}O₂. In this two-step procedure, the compositions of Pd, Nb, and Ti in the support material

could be adjusted to form different materials containing different amounts of these metals. However, for Nb–doped TiO_2 , the mole compositions for Nb and Ti were kept constant at 0.06 and 0.94, respectively. Therefore, for the Nb–doped TiO_2 sample, the molecular expression, $\text{Nb}_{0.06}\text{Ti}_{0.94}\text{O}_2$, is used in this paper, indicating that the sum of the mole composition of Nb and Ti is equal to one. For the Pd composite with $\text{Nb}_{0.06}\text{Ti}_{0.94}\text{O}_2$, weight percentage is used. The general expression for the composite support can be written as $\text{Pd}_x-(\text{Nb}_{0.06}\text{Ti}_{0.94}\text{O}_2)_y$, where x and y are the weight percentages of Pd and $\text{Nb}_{0.06}\text{Ti}_{0.94}\text{O}_2$ in the composite, respectively. In the case of the support alone, the sum of x and y should be equal to 100 wt%. In this work, three composites were synthesized with $x = 10, 30$, or 50 wt%, and the corresponding $y = 90, 70$, and 50 wt%, respectively. The corresponding supports can be expressed as: $\text{Pd}_{10\text{wt}\%}-(\text{Nb}_{0.06}\text{Ti}_{0.94}\text{O}_2)_{90\text{wt}\%}$, $\text{Pd}_{30\text{wt}\%}-(\text{Nb}_{0.06}\text{Ti}_{0.94}\text{O}_2)_{70\text{wt}\%}$, and $\text{Pd}_{50\text{wt}\%}-(\text{Nb}_{0.06}\text{Ti}_{0.94}\text{O}_2)_{50\text{wt}\%}$, respectively.

2.3. Catalyst synthesis

In this paper, the weight percentage of the Pt–Pd catalyst alloy in the supported catalysts was fixed at 20 wt%. For the catalyst synthesis, 90 mg of support material was first ultrasonicated in ethylene glycol (20 ml) for 1 h, and then a mixture Pt–Pd solution, which was prepared by mixing a $(\text{NH}_4)_2\text{PdCl}_6$ solution containing 18.9 mg $(\text{NH}_4)_2\text{PdCl}_6$ with the solvents of 0.5 ml DI water and 1 ml ethylene glycol, and a $\text{H}_2\text{PtCl}_6 \cdot 6\text{H}_2\text{O}$ solution containing 45.25 mg $\text{H}_2\text{PtCl}_6 \cdot 6\text{H}_2\text{O}$ and 0.5 ml DI water, was added dropwise into the above support material containing solution while stirring. After that, a solution of 0.1 M NaOH was added to control the pH at 10. After a few minutes of mixing, the beaker was placed in the center of a microwave oven (Sonicator 3000, Misonix) and heated for 120 s. The resulting suspension was filtered and the residue was washed with DI water three times. The solid product was dried at 60 °C overnight in an oven to obtain the final supported alloy catalyst. Three supported alloy catalysts were formed, 20 wt% $\text{Pt}_{0.62}\text{Pd}_{0.38}/\text{Pd}_{10\text{wt}\%}-(\text{Nb}_{0.06}\text{Ti}_{0.94}\text{O}_2)_{90\text{wt}\%}$, 20 wt% $\text{Pt}_{0.62}\text{Pd}_{0.38}/\text{Pd}_{30\text{wt}\%}-(\text{Nb}_{0.06}\text{Ti}_{0.94}\text{O}_2)_{70\text{wt}\%}$, and 20 wt% $\text{Pt}_{0.62}\text{Pd}_{0.38}/\text{Pd}_{50\text{wt}\%}-(\text{Nb}_{0.06}\text{Ti}_{0.94}\text{O}_2)_{50\text{wt}\%}$, respectively.

For the Pt–Pd alloy catalyst in these supported catalysts, the mole ratio of Pt: Pd is 62:38. As discussed in a later section, catalysts with two other Pt: Pd ratios (15:85, 35:65) were also synthesized in an effort to optimize the ORR activity. Note that for these supported catalysts, the weight percentage of platinum/palladium alloy catalyst for each one is 20 wt%, and the support accounts for 80 wt%.

2.4. Physical characterization

For chemical stability of the support, a typical sample ($\text{Pd}_{30\text{wt}\%}-(\text{Nb}_{0.06}\text{Ti}_{0.94}\text{O}_2)_{70\text{wt}\%}$) synthesized by the two-step procedure was tested in an acid solution. 200 mg of the sample was added into 50 ml of 1 M H_2SO_4 , and heated at 95 °C for 24 h or at 200 °C for 2 h, respectively. The sample's ion concentration in the solution was analyzed by inductively coupled plasma mass spectrometry (ICP-MS) to obtain its solubility.

The electronic conductivity of the support materials was determined using the electrochemical impedance spectroscopy (EIS) method at room temperature. For preparing the sample pellet, 87.3 kPa of pressure was used to press the sample powder into a pellet. The EIS measurements were carried out using a Solartron 1260 frequency response analyzer (FRA) connected to a Solartron 1480A Multistat over the frequency range from 100 kHz to 0.1 Hz with a 10 mV AC perturbation.

For composition of the support materials and their supported Pt–Pd alloy catalysts, powder X-ray diffraction (XRD), using a Bruker D8 Advanced X-ray diffractometer with Cu $K\alpha$ radiation ($\lambda = 1.5406$ Å), was used at a scan rate of 0.02°s^{-1} in the 2θ range from 10° to 90° . The morphology and dispersion of the catalyst nanoparticles on the support material were examined using a conventional transmission electron microscope (TEM, Philips CM12) at relatively low magnification. Samples for TEM observation were directly supported on a copper mesh with a carbon microgrid. STEM HAADF images were acquired using a scanned focused probe together with a high-angle annular dark field detector on the FEI Titan 80–300 Cubed TEM operated at 300 kV. The instrument was equipped with a Gatan Imaging Filter (GIF) for an energy dispersive X-ray detector for elemental analysis and mappings.

Surface-area determination was carried out with the Brannauer–Emmet–Teller (BET) technique using a Beckman Coulter analyzer (Model SA3100).

2.5. Electrochemical characterization

For electrochemical characterization, the working electrodes were coated with the supported catalyst using the following procedure: A catalyst ink was prepared by mixing 18.9 mg of the sample powder with 9.5 ml of distilled water and 0.5 ml of isopropyl alcohol under sonication for 1 h. Then 24 μl of this ink was placed onto a pre-cleaned glassy carbon (GC) electrode. After solvent evaporation, the deposited coating layer was covered with 7 μl of Nafion® ionomer solution (5 wt%, Dupont) in order to fix the particles on the GC surface. This coated electrode was then dried in air for 0.5 h, followed by electrochemical measurements using a rotating disk electrode (RDE) method. A Pine three-electrode cell (rotating disk working electrode, a reversible hydrogen reference electrode (RHE), and a Pt wire counter electrode) was used for all electrochemical measurements. For surface electrochemical measurements, cyclic voltammograms (CVs) (20 cycles at a potential rate of 20 mV s^{-1} in the potential range of 0.05–1.2 V (RHE)) of the coated electrode were recorded in a N_2 -purged 0.1 M HClO_4 electrolyte. For ORR measurements, linear current–voltage curves of the catalyst-coated electrode were measured at a potential scan rate of 5 mV s^{-1} and an electrode rotation rate of 1600 rpm in an O_2 -saturated 0.1 M HClO_4 electrolyte solution. All electrochemical experiments were performed at 31 °C and ambient pressure using a Solartron multichannel potentiostat model 1480 (controlled with Corrware software, Scribner Associates Inc., USA).

3. Results and discussion

3.1. Chemical stability of the support materials

In this approach, the major purpose in developing metal oxide support materials is to replace carbon as a high temperature PEM fuel cell catalyst support which can operate in an acidic environment in the temperature range from 90 to 200 °C. Therefore, the stability of the support becomes an important criterion for judging its feasibility. In this experiment, the chemical stability was estimated by measuring the materials' solubility in acidic solution at both the temperatures of 95 °C and 200 °C. $\text{Pd}_{30\text{wt}\%}-(\text{Nb}_{0.06}\text{Ti}_{0.94}\text{O}_2)_{70\text{wt}\%}$ was chosen as the example support for testing. After the sample was individually exposed to acidic solution at these two temperatures, the solutions were analyzed using the ICP-MS method to obtain the weights of dissolution. In this way, the weight loss percentages could be calculated and are shown in Fig. 1. It can be seen that the weight losses at the two

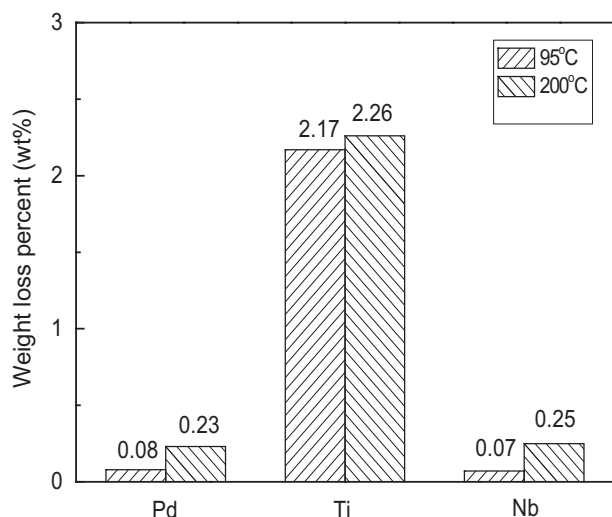


Fig. 1. Weight losses of Pd, Ti and Nb in the sample (Pd_{30wt%}–(Nb_{0.06}Ti_{0.94}O₂)_{70wt%}) after chemical stability test in 1 M H₂SO₄ at 95 °C and 200 °C, respectively.

temperatures for all metals are less than 3 wt%, demonstrating that this material is chemically stable when a 5 wt% loss is set as the tolerance limit.

3.2. BET surface area and conductivity of the supports

The BET surface areas for various Pd–composited Nb_{0.06}Ti_{0.94}O₂ samples were measured, as shown in Table 1. All BET surface areas are much smaller (<12 m² g^{−1}) than those of carbon support materials. For example, a typical commercially available carbon support has a BET surface area of 866 m² g^{−1}. Compared to pure Nb_{0.06}Ti_{0.94}O₂, the Pd–composite Nb_{0.06}Ti_{0.94}O₂ samples have slightly higher BET surface areas. Although BET surface area is not the main focus of this paper, it can affect the catalyst deposition, and dispersion as well as the catalyst activity, which will be further investigated in our continuing work.

Electronic conductivities of support materials for fuel cell catalyst applications are required to be higher than 0.1 S cm^{−1} [21,22]. This is because more highly conductive supports favor the electron transfer between the platinum particle and the support [30,31]. Table 1 lists the conductivities of all samples. It can be seen that the conductivity can be increased from 8.9×10^{-2} S cm^{−1} to 2.65 S cm^{−1} with increasing the Pd content from 10 wt% to 50 wt% while the pure Nb_{0.06}Ti_{0.94}O₂ has a low conductivity of 4.45×10^{-3} S cm^{−1}. The increase of conductivity can be mainly attributed to the addition of Pd in the Pd–composite Nb_{0.06}Ti_{0.94}O₂. According to the literature [32–35], the electronic conducting paths can be generated by metallic clusters in contact. When particles touch each other, space charges are created and the Fermi energies are equilibrated [36–38]. The migration of charge carriers from one material to

the other can lead to an energy band distortion, and as a consequence, some electrons (or holes) can occupy energy states in the conduction band (or valence band), and migrate through the material by percolation. The percolation through touching metal particles is not identical with that through overlapping space charge layers [39].

3.3. XRD characterization

Fig. 2 shows the powder XRD patterns of different Pd–composite Nb_{0.06}Ti_{0.94}O₂ samples and their corresponding Pt–Pd alloy catalysts. The XRD patterns of the Pd–Nb_{0.06}Ti_{0.94}O₂ composite samples show the separate phases of Pd (dark circle) and rutile TiO₂ (open circle) for Nb_{0.06}Ti_{0.94}O₂. However, no distinct niobium oxide phases can be found for Nb_{0.06}Ti_{0.94}O₂ in Fig. 2a due to either its amorphous structure in Nb–doped TiO₂ at low mole percentages [40] or due to the easy doping of rutile TiO₂ with Nb [41]. The formation of a pure rutile TiO₂ (open circle) for Nb_{0.06}Ti_{0.94}O₂ can also be seen because the samples were reduced at 700 °C for 10 h in H₂. This temperature of 700 °C is the transition temperature for TiO₂ from the anatase to rutile phase [25,42]. From the XRD patterns, the Pd crystallite size

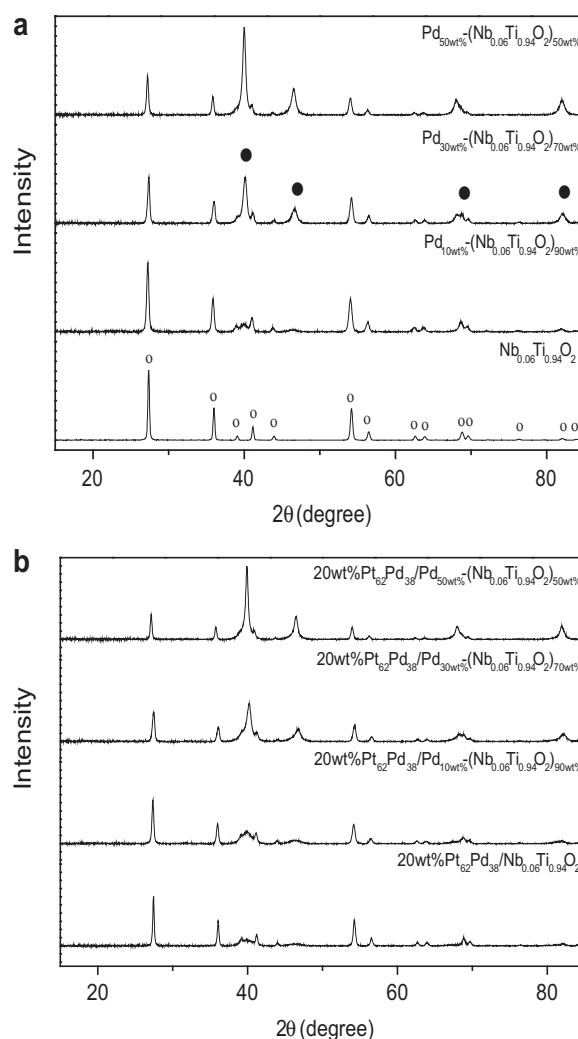


Fig. 2. X-ray diffraction patterns for (a) Nb_{0.06}Ti_{0.94}O₂ and Pd–Nb_{0.06}Ti_{0.94}O₂ composite materials with various Pd content, and (b) their corresponding supported Pt–Pd catalysts.

Table 1
Conductivities and BET surface areas for Nb_{0.06}Ti_{0.94}O₂, and various Pd–Nb_{0.06}Ti_{0.94}O₂ composite supports.

Sample	Conductivity (S cm ^{−1})	BET (m ² g ^{−1})
Nb _{0.06} Ti _{0.94} O ₂	4.45×10^{-3}	4.5
Pd _{10wt%} –(Nb _{0.06} Ti _{0.94} O ₂) _{90wt%}	8.92×10^{-2}	5.5
Pd _{30wt%} –(Nb _{0.06} Ti _{0.94} O ₂) _{70wt%}	4.81×10^{-1}	10.4
Pd _{50wt%} –(Nb _{0.06} Ti _{0.94} O ₂) _{50wt%}	2.65	9.0

Table 2
Crystallite size of Pd in various Pd–Nb_{0.06}Ti_{0.94}O₂ composite supports.

Sample	Crystallite size (nm)
Pd _{10wt%} –(Nb _{0.06} Ti _{0.94} O ₂) _{90wt%}	6.6
Pd _{30wt%} –(Nb _{0.06} Ti _{0.94} O ₂) _{70wt%}	11.3
Pd _{50wt%} –(Nb _{0.06} Ti _{0.94} O ₂) _{50wt%}	12.9

was calculated using the Debye–Scherrer equation [43] and is presented in Table 2. It can be seen that for Pd–Nb_{0.06}Ti_{0.94}O₂ composite samples, the Pd crystallite size increases with increasing Pd content. The XRD pattern of the Pd-composite supported Pt–Pd catalysts, synthesized by the microwave assisted polyol method [44,45], was also recorded and are shown in Fig. 2b. After the dispersion of the PtPd alloy, the PtPd alloy peaks were overlapped by Pd peaks from the Pd–Nb_{0.06}Ti_{0.94}O₂ support. What is more, the intensity and position of the PtPd peaks for the catalysts (see Fig. 2b) are almost the same as that for the Pd peaks from their corresponding supports (see Fig. 2a). Whether it is the support or the supported PtPd catalyst, the intensity of the PtPd peak is found to increase with increasing Pd content inside the Pd–Nb_{0.06}Ti_{0.94}O₂ support. To estimate the actual composition for all the alloy catalyst in Fig. 2a, Vegard's law [46,47] was used in the calculation. The lattice parameters and the atomic fractions of Pt alloyed in the catalyst are listed in Table 3. It can be seen that based on these lattice parameters, the calculated Pt atomic fraction of 20 wt% Pt_{0.62}Pd_{0.38}/Nb_{0.06}Ti_{0.94}O₂ is 0.621, which is in good agreement with the nominal value (~0.62). After the addition of pure Pd introduced into the support, the catalyst has a decreased Pt atomic fraction, suggesting that much more Pd took part in the formation of Pt–Pd alloy, and thus these alloys probably favor increased electrochemical catalytic activity.

3.4. TEM and EELS characterization

For the Pd–Nb_{0.06}Ti_{0.94}O₂ composite materials, TEM-EDX was used to characterize the effect of Pd on the morphology of Nb_{0.06}Ti_{0.94}O₂ at the microscale. Fig. 3a shows a TEM image of the Pd_{30wt%}–(Nb_{0.06}Ti_{0.94}O₂)_{70wt%} sample. Two EDX spectra shown in Fig. 3b were acquired at the two points labeled in Fig. 3a as SP1 and SP2, respectively. It can be seen that the EDX spectrum in area SP1 does not show a significant Pd peak, but only Ti, Nb and O peaks, suggesting that the larger particle is mainly composed of Nb_{0.06}Ti_{0.94}O₂. However, the spectrum from area SP2 shows clear characteristic peaks of Ti, Nb, O and Pd, suggesting that Pd particles are only formed on the surface of the Nb_{0.06}Ti_{0.94}O₂ support during the two-step synthesis. Fig. 3c shows that the Pd particle size distribution is mainly in the range of 10–15 nm.

For the Pt–Pd alloy catalyst supported on the Pd–Nb_{0.06}Ti_{0.94}O₂ composite, TEM imaging and a particle size distribution

Table 3
Pt alloy lattice parameters and atomic fractions for the supported catalysts: 20 wt% Pt_{0.62}Pd_{0.38}/Nb_{0.06}Ti_{0.94}O₂, 20 wt% Pt_{0.62}Pd_{0.38}/Pd_{10wt%}–(Nb_{0.06}Ti_{0.94}O₂)_{90wt%}, 20 wt% Pt_{0.62}Pd_{0.38}/Pd_{30wt%}–(Nb_{0.06}Ti_{0.94}O₂)_{70wt%}, and 20 wt% Pt_{0.62}Pd_{0.38}/Pd_{50wt%}–(Nb_{0.06}Ti_{0.94}O₂)_{50wt%}.

Catalyst	Lattice parameter calculated (nm)	Pt atomic fraction in PtPd alloy
20 wt% Pt _{0.62} Pd _{0.38} /Nb _{0.06} Ti _{0.94} O ₂	0.39149	0.621
20 wt% Pt _{0.62} Pd _{0.38} /Pd _{10wt%} –(Nb _{0.06} Ti _{0.94} O ₂) _{90wt%}	0.39121	0.505
20 wt% Pt _{0.62} Pd _{0.38} /Pd _{30wt%} –(Nb _{0.06} Ti _{0.94} O ₂) _{70wt%}	0.39097	0.404
20 wt% Pt _{0.62} Pd _{0.38} /Pd _{50wt%} –(Nb _{0.06} Ti _{0.94} O ₂) _{50wt%}	0.39067	0.279

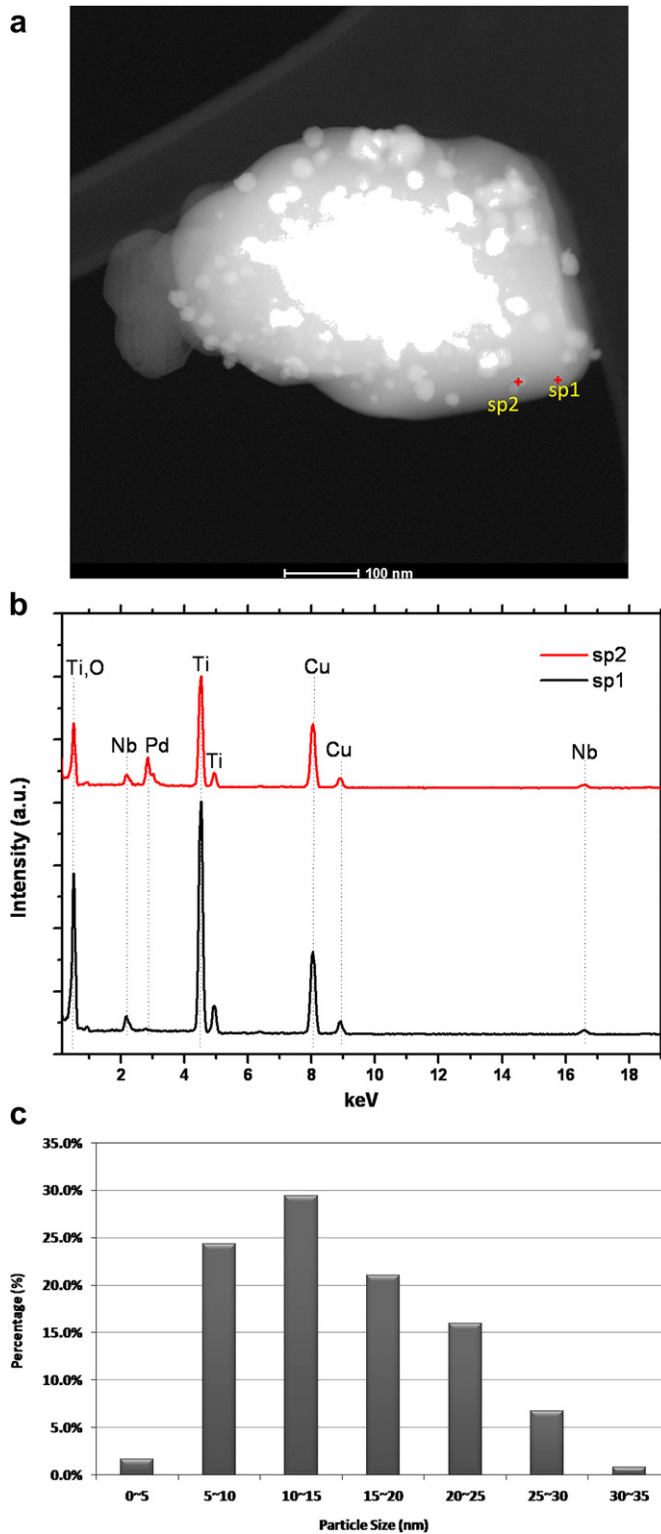


Fig. 3. STEM image (a), EDX spectra (b), and Pd particles size distribution (c) for Pd_{30wt%}–(Nb_{0.06}Ti_{0.94}O₂)_{70wt%} support synthesized by the two-step method.

measurement of a typical 20 wt% Pt_{0.62}Pd_{0.38}/Pd_{30wt%}–(Nb_{0.06}Ti_{0.94}O₂)_{70wt%} catalyst was conducted and the results are shown in Fig. 4. As shown in Fig. 4c, the catalyst exhibits a particle size distribution on the support mainly in the range of 3–4 nm. Considering the Pd particle size range of 10–15 nm on the support in Fig. 3c, it can be inferred that the smaller particles in

Fig. 4c should be the Pt–Pd alloy particles obtained via the microwave assisted reduction method.

To further characterize the morphology of the catalysts, data from a high-angle-annular-dark-field image from scanning-transmission electron microscopy (HAADF-STEM) was also collected for the 20 wt% Pt_{0.62}Pd_{0.38}/Pd_{30wt%}–(Nb_{0.06}Ti_{0.94}O₂)_{70wt%} catalyst sample. Fig. 5a shows two types of particles with different sizes on a large metal oxide particle. One type of particle is composed of clusters below 5 nm in size while the other type contains larger particles with sizes up to 10 nm. Point EDX spectra generated from various locations in the sample (Fig. 5b) further indicate the variation of the chemical composition within the different areas of the catalyst/sample. The square area highlighted in Fig. 5a presents the corresponding region where EDX mapping was performed. The peak assigned to Cu in the EDX spectra can be attributed to the grid used for the TEM measurement. It can be seen that all of the elements (Ti, Nb, O, Pd, and Pt) are present in the regions identified as SP1 and SP2, while SP3 from the surface of the dark large metal oxide particle with a size of ~100 nm does not give any clear Pd peak. This result indicates that for the catalyst with the two-step synthesized support, the Pd particles and Pt–Pd alloy are formed on the surface of the support materials rather than inside the oxide, as confirmed by EDX mapping results shown in Fig. 5c. The distribution of Ti, O, and Nb are almost uniform in Fig. 5c.

Thus, three distinct phase areas, pure Pd, the PtPd alloy and the Nb–doped TiO₂ particle all exist in the catalyst sample, which may provide some connection among them and produce a close relationship in physiochemical properties, possibly favoring the improvement of electrochemical performance.

3.5. Surface electrochemistry of supports and their supported Pt–Pd alloy catalysts

3.5.1. Surface electrochemistry of the catalysts

To evaluate the electrocatalytic properties of the Pt–Pd alloy catalysts supported on the Pd–Nb_{0.06}Ti_{0.94}O₂ composite, their cyclic voltammograms (CV) were recorded at 31 °C in N₂-purged 0.1 M HClO₄ solution at a sweep rate of 20 mV s^{−1}, as shown in Fig. 6. The CV curves exhibit two typical potential regions, one associated with H adsorption/desorption processes ($H^+ + e^- \leftrightarrow H$) between 0 and 0.4 V, and the other with the formation of a PtO layer ($PtO + 2e^- + 2H^+ \leftrightarrow Pt + H_2O$) beyond ~0.6 V if the catalyst is pure Pt or supported Pt. For the Pd-containing catalysts, the sharp peak at the left end of the curves is mainly from those hydrogen atoms which penetrate inside the bulk Pd. Therefore, the peaks in the hydrogen adsorption–desorption region, which are associated with bonded hydrogen species on Pt and on or inside the Pd metal [48–52], may be integrated to determine the quantity

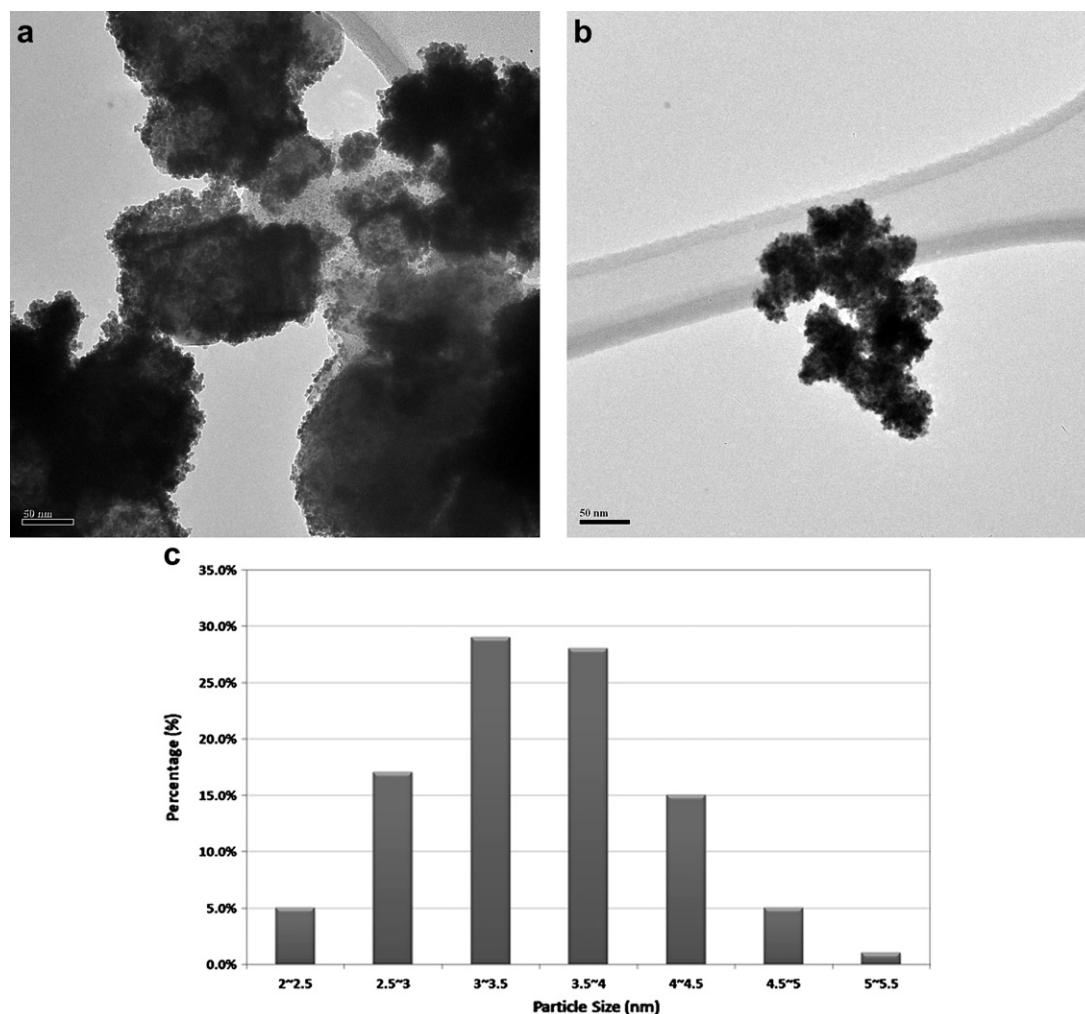


Fig. 4. TEM bright-field image (a, b) and size distribution of Pt–Pd alloy particle (c) for 20 wt% Pt₆₂Pd₃₈/Pd_{30wt%}–(Nb_{0.06}Ti_{0.94}O₂)_{70wt%} catalyst.

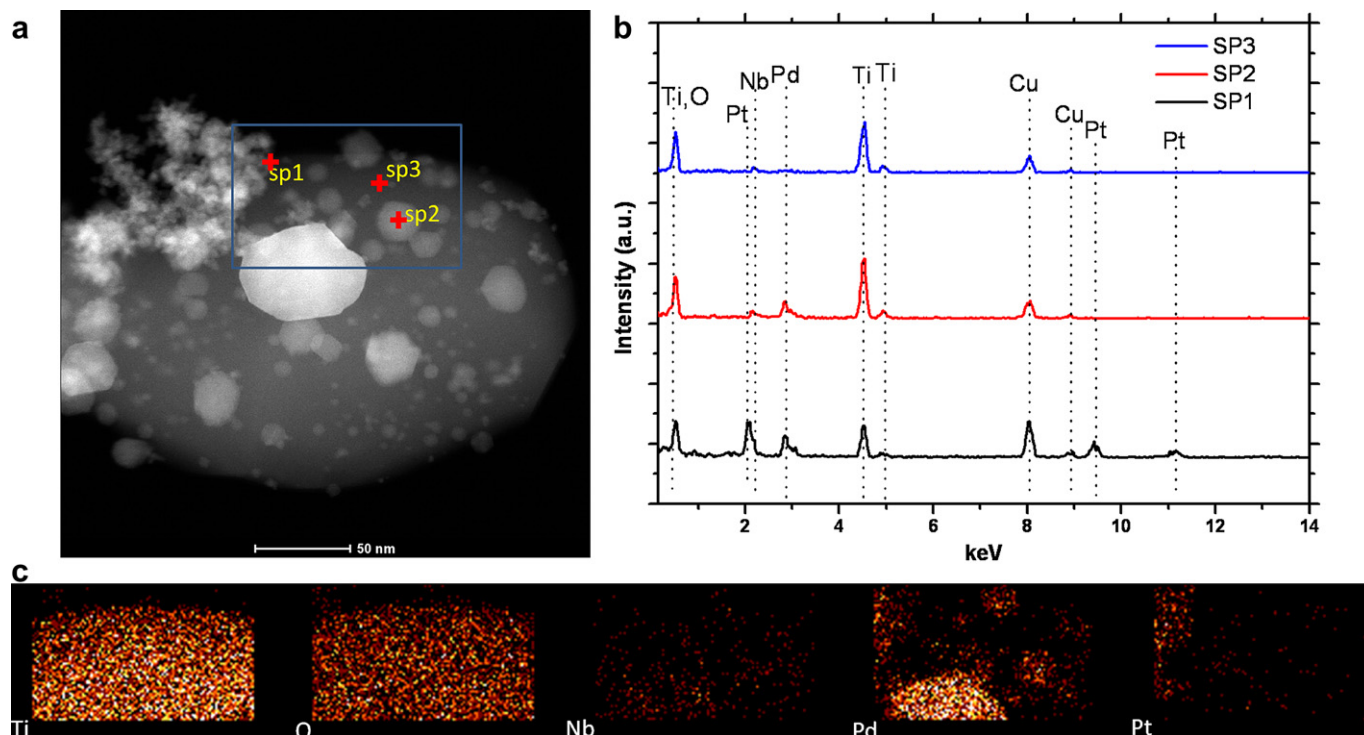


Fig. 5. (a) STEM-HAADF image, (b) EDX point spectra from locations SP1, SP2 and SP3 identified from the HAADF-STEM image, and (c) EDXS elemental mapping from different locations shown in the HAADF-STEM image for the 20 wt% $\text{Pt}_{0.62}\text{Pd}_{0.38}/\text{Pd}_{30\text{wt}\%}-(\text{Nb}_{0.06}\text{Ti}_{0.94}\text{O}_2)_{70\text{wt}\%}$ catalyst.

of hydrogen involved, but are not adequate for the evaluation of the electrochemical surface area (ECSA) of these catalysts [48–52]. Unfortunately, the accepted method of determining ECSA through hydrogen electrochemical adsorption/desorption is only appropriate for pure Pt or supported pure Pt catalyst rather than Pt alloy-based catalysts. However, according to Schmidt et al. [53], an alternative method using CO adsorption/desorption could be considered to estimate the ECSA. At the time of this manuscript, the authors are performing such CO adsorption/desorption measurements. Discussion of these results is the subject of future work.

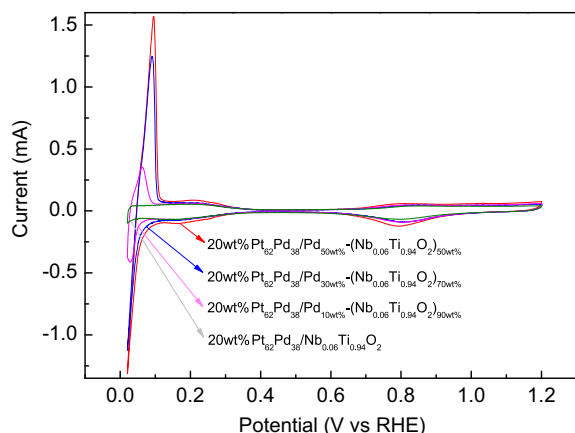


Fig. 6. Cyclic voltammograms for the 20 wt% $\text{Pt}_{0.62}\text{Pd}_{0.38}/\text{Pd}_x-(\text{Nb}_{0.06}\text{Ti}_{0.94}\text{O}_2)_{100-x}$ catalyst series, recorded at 31 °C in an N_2 -purged 0.1 M HClO_4 solution with a potential scan rate of 20 mV s^{-1} . The catalyst loading on the glassy carbon rotating disk electrode is 46.2 $\mu\text{g cm}^{-2}$.

3.5.2. Oxygen reduction reaction (ORR) activity

ORR activity of Pt-based bimetallic electrocatalysts is one of the more important electrochemical properties to evaluate. Recently, a lot of research has been reported to improve the catalytic activity of Pt_xM_y ($\text{M} = \text{Co}, \text{Cu}, \text{Pd}, \text{Ir}, \text{Ni}, \text{Au}$) bimetallic electrocatalysts [54–58]. These bimetallic catalysts could be favorable candidates in the development of active ORR catalysts on non-carbon supports. To investigate the ORR activity of the Pd–Pt alloy catalysts supported on $\text{Nb}_{0.06}\text{Ti}_{0.94}\text{O}_2$ and the Pd– $\text{Nb}_{0.06}\text{Ti}_{0.94}\text{O}_2$ composite, rotating disk electrodes individually coated with four different catalysts (20 wt% $\text{Pt}_{0.62}\text{Pd}_{0.38}/\text{Nb}_{0.06}\text{Ti}_{0.94}\text{O}_2$, 20 wt% $\text{Pt}_{0.62}\text{Pd}_{0.38}/\text{Pd}_{10\text{wt}\%}-(\text{Nb}_{0.06}\text{Ti}_{0.94}\text{O}_2)_{90\text{wt}\%}$, 20 wt% $\text{Pt}_{0.62}\text{Pd}_{0.38}/\text{Pd}_{30\text{wt}\%}-(\text{Nb}_{0.06}\text{Ti}_{0.94}\text{O}_2)_{70\text{wt}\%}$, and 20 wt% $\text{Pt}_{0.62}\text{Pd}_{0.38}/\text{Pd}_{50\text{wt}\%}-(\text{Nb}_{0.06}\text{Ti}_{0.94}\text{O}_2)_{50\text{wt}\%}$) were measured at a rotating speed of 1600 rpm in an O_2 -saturated 0.1 M HClO_4 solution, and the obtained current–voltage curves are shown in Fig. 7(a) and (b). Fig. 7(c) exhibits the ORR current–voltage curves for $\text{Pd}_{30\text{wt}\%}-(\text{Nb}_{0.06}\text{Ti}_{0.94}\text{O}_2)_{70\text{wt}\%}$ and 20 wt% $\text{Pt}/[\text{Pd}_{30\text{wt}\%}-(\text{Nb}_{0.06}\text{Ti}_{0.94}\text{O}_2)_{70\text{wt}\%}]$. It can be seen that various catalysts have different ORR activities. For a more quantitative estimation of the ORR activity, the Koutecky–Levich theory can be used to express the disk current in terms of kinetics and diffusion [59,60]:

$$\frac{1}{j} = \frac{1}{j_k} + \frac{1}{j_d} + \frac{1}{j_f} \quad (1)$$

where j is the measured disk current density, j_k is the kinetic current density, j_d is the diffusion limiting current density, and j_f is the diffusion-limited current density through the Nafion® film [61].

If the thickness of the Nafion® film used to bind the catalysts on the electrode is thin enough the term $1/j_f$ in Equation (1) can be considered negligible [62]. As a result, Equation (1) can be simplified to Equation (2):

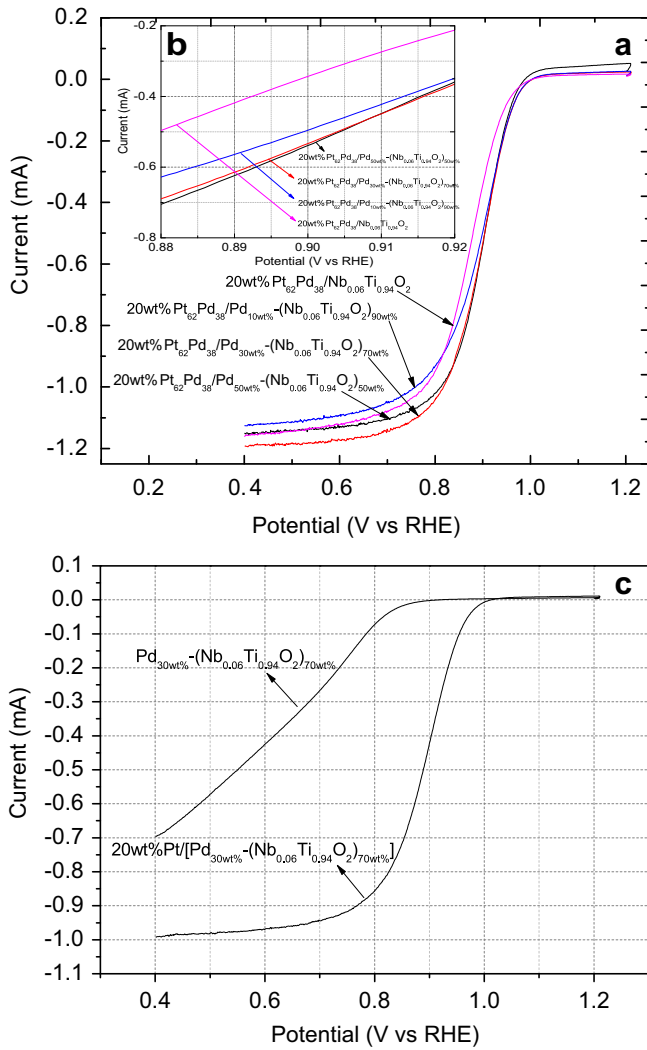


Fig. 7. ORR linear sweep voltammogram recorded on the supported catalyst: 20 wt% Pt_{0.62}Pd_{0.38}/Nb_{0.06}Ti_{0.94}O₂, 20 wt% Pt_{0.62}Pd_{0.38}/Pd_{10wt%}-(Nb_{0.06}Ti_{0.94}O₂)_{90wt%}, 20 wt% Pt_{0.62}Pd_{0.38}/Pd_{30wt%}-(Nb_{0.06}Ti_{0.94}O₂)_{70wt%}, 20 wt% Pt_{0.62}Pd_{0.38}/Pd_{50wt%}-(Nb_{0.06}Ti_{0.94}O₂)_{50wt%}, Pd_{30wt%}-(Nb_{0.06}Ti_{0.94}O₂)_{70wt%}, and 20 wt% Pt/[Pd_{30wt%}-(Nb_{0.06}Ti_{0.94}O₂)_{70wt%}], respectively at 31 °C in a O₂-saturated 0.1 M HClO₄ solution. The electrode rotation rate was 1600 rpm, and the potential scan rate was 5 mV s⁻¹. The catalyst loading on the glassy carbon RDE was 46.2 μg cm⁻².

$$\frac{1}{j} = \frac{1}{j_k} + \frac{1}{j_d} \quad (2)$$

The j_d term in Equation (2) can also be expressed by Equation (3):

$$j_d = 0.62nFD_0^{2/3}C_{O_2}v^{-1/6}\omega^{1/2} \quad (3)$$

where n is the number of overall electrons transferred, ω is the electrode rotation rate, F is the Faraday constant (96,485 C mol⁻¹), D_{O_2} is the diffusion coefficient of O₂ in 0.1 M HClO₄ solution (1.9 × 10⁻⁵ cm² s⁻¹), C_{O_2} is the saturation concentration of oxygen in 0.1 M HClO₄ solution (1.13 × 10⁻⁶ mol cm⁻³) [63], and v is the kinematic viscosity (0.010 cm² s⁻¹). At 1600 rpm, j and j_k values can be derived from Equation (2) with the measured geometric current density values from Fig. 7. Fig. 8 displays the trends for the mass activities as a function of Pd content in the support. It can be seen that when Pd forms a composite with the Nb_{0.06}Ti_{0.94}O₂ support, all

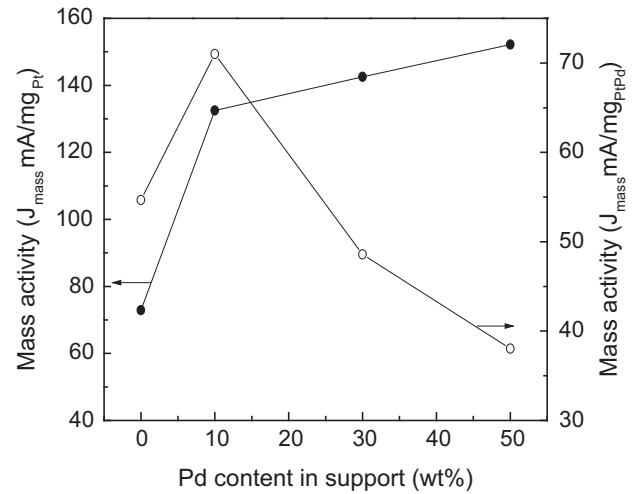


Fig. 8. ORR mass activities of the supported Pt–Pd alloy catalysts as a function of Pd content in the Nb_{0.06}Ti_{0.94}O₂ support.

supported Pt–Pd alloy catalysts exhibit higher ORR mass activities than for the case without Pd in the support and commercial 47 wt% Pt/TKKE (Based on the recorded ORR current–voltage curves in Fig. 9, its calculated Pt ORR mass activity is 102 mA mg_{Pt}⁻¹). However, the Pt–Pd mass activity decreases beyond 10 wt% Pd in the support with increasing Pd support content. Pd is not active toward the ORR and therefore dilution of the Pt content with Pd would be expected to decrease mass activity at some point with respect to the Pt–Pd alloy composition. As shown in Fig. 7(c), the Pd_{30wt%}-(Nb_{0.06}Ti_{0.94}O₂)_{70wt%} support material and 20 wt% Pt/[Pd_{30wt%}-(Nb_{0.06}Ti_{0.94}O₂)_{70wt%}] catalyst have low ORR current at an electrode rotation rate of 1600 rpm, and a potential scan rate of 5 mV s⁻¹. The calculated Pt ORR mass activity of the Pd_{30wt%}-(Nb_{0.06}Ti_{0.94}O₂)_{70wt%} is 3.015 × 10⁻⁴ mA mg_{Pd}⁻¹ while the 20 wt% Pt/[Pd_{30wt%}-(Nb_{0.06}Ti_{0.94}O₂)_{70wt%}] catalyst have a Pt ORR mass activity around 78 mA mg_{Pt}⁻¹, lower than those of 20 wt% Pt_{0.62}Pd_{0.38}/[Pd_{30wt%}-(Nb_{0.06}Ti_{0.94}O₂)_{70wt%}] and the commercial Pt/C catalyst. This suggests a very low contribution of Pd on the ORR mass activity of the Pd_{30wt%}-(Nb_{0.06}Ti_{0.94}O₂)_{70wt%} support.

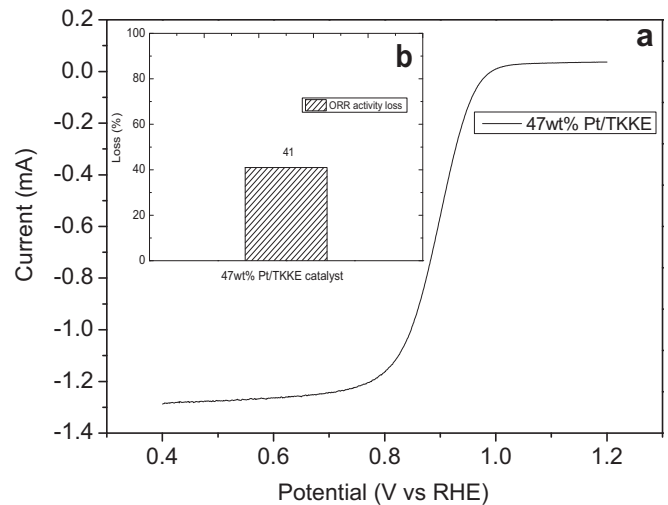


Fig. 9. (a) The ORR current–voltage curves and (b) Pt ORR mass activity loss data of commercial 47 wt% Pt/TKKE catalyst.

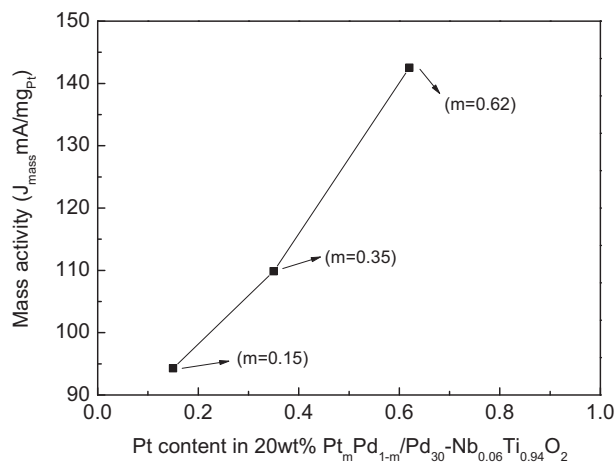


Fig. 10. ORR mass activity of 20 wt% Pt_mPd_{1-m}/Pd_{30wt%}-(Nb_{0.06}Ti_{0.94}O₂)_{70wt%} as a function of Pt mole content (*m*) in the catalysts.

The enhanced Pt mass activity with increasing Pd content in the support may be due to the formation of Pt–Pd clusters on the support surface. According to the STEM results in Figs. 3 and 5, some pure Pd can be observed on the Nb_{0.06}Ti_{0.94}O₂ support. After the Pt–Pd alloy is deposited on the support, there may be some Pt–Pd particles deposited on pure Pd to form Pt_mPd_n clusters. The calculated alloy composition in Table 3 shows a different change when the various Pd content was added to the support, suggesting the formation of Pt_mPd_n clusters. Theoretically, in the presence of Pd, Density Functional Theory (DFT) calculations predict that the Pt atom bears negative charges while the Pd atom bears positive charges in the Pt_mPd_n clusters, and that the negatively charged Pt atoms in Pt_mPd_n can facilitate the dissociation of O₂ on the Pt surface, thus enhancing ORR activity [64]. In the work here, at high Pd content, there should be more pure Pd distributed on the Nb_{0.06}Ti_{0.94}O₂ support surface during the two-steps synthesis. As a result, more Pt_mPd_n clusters are likely formed on the support after the Pt–Pd alloy deposition, leading to higher Pt mass activity. In the oxygen reduction reaction, the generally accepted four-electron transfer mechanism involves O–O bond breaking and O–H bond formation at the catalyst surface. It can be inferred that with increasing Pd content, the catalyst in the presence of alloy composite like Pt–M (M = Pd) becomes more effective in binding oxygen strongly enough to break the O–O bond while binding the OH group only moderately such that OH removal from the catalyst surface by water elimination is reasonably facile [55,57,58]. Another factor enhancing the ORR activity with increasing Pd content in the support would be the increased electronic conductivity as shown in Table 1. The support with high conductivity favors the electron transfer between the Pt–Pd alloy particles and the Pd–Nb_{0.06}Ti_{0.94}O₂ composite support, which can promote the dissociation of O₂ on the Pt surface and correspondingly contribute to the improvement of ORR activity.

Regarding the effect of Pt content in the catalysts, Pt–Pd alloy catalysts with different mole ratios of Pt and Pd were also synthesized in this paper. Fig. 10 shows the ORR mass activities as a function of Pt mole content in the catalyst. It can be clearly observed that with increasing Pt molar content (*m*), the Pt_mPd_{1-m}/Pd_{30wt%}-(Nb_{0.06}Ti_{0.94}O₂)_{70wt%} catalyst exhibits an increased ORR mass activity. At *m* = 0.15, 0.35, and 0.62, the weight ratio of Pt to Pd in the Pt–Pd alloy is 1:3, 1:1 and 3:1, respectively. The improvement in ORR mass activity is due to the higher Pt content favoring the O–O bond-breaking on the catalyst surface and thus enhancing the ORR mass activity.

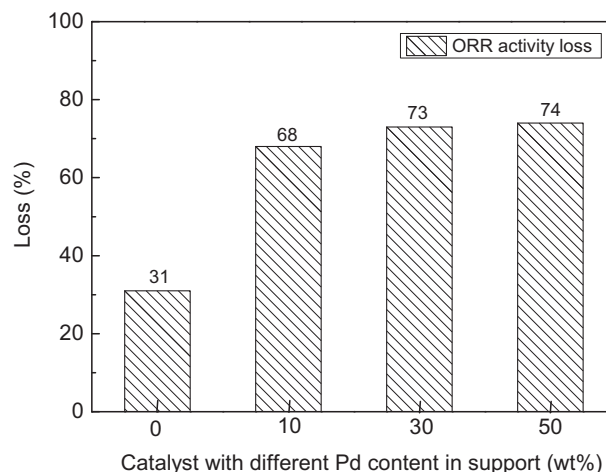


Fig. 11. Pt ORR mass activity losses for several 20 wt% Pt_{0.62}Pd_{0.38}/Pd_{*x*}-(Nb_{0.06}Ti_{0.94}O₂)_{100-*x*} catalysts as a function of Pd content in the Nb_{0.06}Ti_{0.94}O₂ support, measured at 30 °C in an N₂-purged 0.1 M HClO₄ solution for 1000 CV cycles in the potential range between 0 and 1.2 V vs. RHE at a scan rate of 20 mV s⁻¹. The electrode rotation rate in an O₂-saturated 0.1 M HClO₄ solution was 1600 rpm, and the potential scan rate was 5 mV s⁻¹. The catalyst loading on the glassy carbon RDE was 46.2 μg cm⁻².

3.5.3. Catalyst stability

Electrocatalysts were evaluated for durability by repeating 1000 CV cycles in the potential range between 0 and 1.2 V vs. RHE at a scan rate of 20 mV s⁻¹ at 30 °C. The electrolyte used was a N₂-purged 0.1 M HClO₄ solution. The activities of all catalyst samples before and after the durability test were measured in an O₂-purged 0.1 M HClO₄ solution at 30 °C. Fig. 11 shows the Pt ORR activity loss of all catalysts as a function of different Pd content. The increase of Pd content in the Nb_{0.06}Ti_{0.94}O₂ support appears to slightly increase the ORR activity loss, suggesting that the Pd–Nb_{0.06}Ti_{0.94}O₂ composite supports have some electrochemical instability in acidic solution. This results in some cases in an ORR activity loss that can be more than 60%. However, 20 wt% Pt_{0.62}Pd_{0.38}/Nb_{0.06}Ti_{0.94}O₂ showed a lower ORR activity loss around 31% than commercial 47 wt% Pt/TKKE (its ORR activity loss was about 41% as shown in Fig. 9). This major degradation mode is believed to be due to the dissolution of Pd in acidic solution, leading to isolated Pt particles. More work is necessary to clearly identify the degradation mechanisms.

4. Conclusions

In this study, we successfully synthesized several Pd–Nb_{0.06}Ti_{0.94}O₂ composite materials by a two-step procedure, and these materials were employed as the catalyst supports for Pt–Pd alloy catalysts for the PEM fuel cell oxygen reduction reaction (ORR). Several characterization methods such as XRD, EDX, TEM, HAADF, BET, solubility testing, as well as conductivity measurements were used to study these supports and their supported catalysts. HAADF-STEM results showed that for Pd–Nb_{0.06}Ti_{0.94}O₂ composite supports, Pd nanoparticles could stay on the Nb_{0.06}Ti_{0.94}O₂ particle surface, and that for the supported Pt–Pd catalysts, the Pt–Pd nanoparticles could stay on both the Nb_{0.06}Ti_{0.94}O₂ particle-Pd composite surfaces and form Pt–Pd clusters. With respect to chemical stability the Pd–Nb_{0.06}Ti_{0.94}O₂ composite support materials showed low solubility in acidic solution, indicating that they may be feasible support materials for ORR electrocatalysts. The electronic conductivity of Nb_{0.06}Ti_{0.94}O₂ could be greatly improved by forming a composite with Pd. For example, the conductivity was increased

after Pd content was increased from 0 wt% to 50 wt% in the support from $4.45 \times 10^{-3} \text{ S cm}^{-1}$ for $\text{Nb}_{0.06}\text{Ti}_{0.94}\text{O}_2$ to 2.65 S cm^{-1} for $\text{Pd}_{50\text{wt}\%}\text{-(Nb}_{0.06}\text{Ti}_{0.94}\text{O}_2)_{50\text{wt}\%}$.

Three Pt–Pd alloy catalysts supported on a $\text{Pd-Nb}_{0.06}\text{Ti}_{0.94}\text{O}_2$ composite material, 20 wt% $\text{Pt}_{0.62}\text{Pd}_{0.38}/\text{Pd}_{10\text{wt}\%}\text{-(Nb}_{0.06}\text{Ti}_{0.94}\text{O}_2)_{90\text{wt}\%}$, 20 wt% $\text{Pt}_{0.62}\text{Pd}_{0.38}/\text{Pd}_{30\text{wt}\%}\text{-(Nb}_{0.06}\text{Ti}_{0.94}\text{O}_2)_{70\text{wt}\%}$, and 20 wt% $\text{Pt}_{0.62}\text{Pd}_{0.38}/\text{Pd}_{50\text{wt}\%}\text{-(Nb}_{0.06}\text{Ti}_{0.94}\text{O}_2)_{50\text{wt}\%}$, were synthesized and tested using both cyclic voltammetric and rotating disk electrode techniques to determine the ORR mass activity, as well as the electrochemical stability. All three catalysts showed higher Pt ORR mass activity ($>130 \text{ mA mg}_{\text{Pt}}^{-1}$ at 0.9 V vs. RHE) than that of the baseline 47 wt% PtC^{-1} catalyst ($110 \text{ mA mg}_{\text{Pt}}^{-1}$). However, these catalysts showed insufficient electrochemical stability compared to the baseline catalyst. For example, after electrochemical cycling for 1000 cycles in the potential range between 0 and 1.2 V vs. RHE in acidic solution, the loss of ORR mass activity could be as high as 70% likely due to the dissolution of Pd in both the support and Pt–Pd alloy. More work is necessary to improve the electrochemical stability of these Pt–Pd alloy catalysts supported on Pd-composited $\text{Nb}_{0.06}\text{Ti}_{0.94}\text{O}_2$ materials.

Acknowledgments

The authors would like to thank the National Research Council of Canada Institute for Fuel Cell Innovation (NRC-IFCI) and the NRC/NRCAN/NSERC Hydrogen and Fuel Cell Program for their financial support. The authors would also like to acknowledge the contribution from Stephen Campbell (AFCC), Siyu Ye (Ballard) and all members of the NRC and UBC catalyst groups. Feihong Nan and Gianluigi A. Botton are grateful to NSERC for a Strategic Grant supporting this work[10].

References

- [1] S.Y. Huang, P. Ganesan, S. Park, B.N. Popov, J. Am. Chem. Soc. 131 (2009) 13898–13899.
- [2] W. Lubitz, W. Tumas, Chem. Rev. 107 (2007) 3900–3903.
- [3] H.A. Gasteiger, S.S. Kocha, B. Sompalli, F.T. Wagner, Appl. Catal. B 56 (2005) 9–35.
- [4] S.Y. Huang, S.M. Chang, C.L. Lin, C.H. Chen, C.T. Yeh, J. Phys. Chem. B 110 (2006) 23300–23303.
- [5] Y. Shao-Horn, W.C. Sheng, S. Chen, P.J. Ferreira, E.F. Holby, D. Morgan, Top. Catal. 46 (2007) 285–305.
- [6] S.G. Chalk, J.E. Miller, J. Power Sources 159 (2006) 73–80.
- [7] M.S. Wilson, F.H. Garzon, K.E. Sickafus, S. Gottesfeld, J. Electrochem. Soc. 140 (1993) 2872–2877.
- [8] Z. Siroma, K. Ishii, K. Yasuda, Y. Miyazaki, M. Inaba, A. Tasaka, Electrochem. Commun. 7 (2005) 1153–1156.
- [9] S.-Y. Huang, P. Ganesan, B.N. Popov, Appl. Catal. B 96 (2010) 224–231.
- [10] H.R. Colon-Mercado, H. Kim, B.N. Popov, Electrochem. Commun. 6 (2004) 795–799.
- [11] S.Y. Huang, C.M. Chang, C.T. Yeh, J. Catal. 241 (2006) 400–406.
- [12] P.H. Matter, L. Zhang, U.S. Ozkan, J. Catal. 239 (2006) 83–96.
- [13] T. Yoda, H. Uchida, M. Watanabe, Electrochim. Acta 52 (2007) 5997–6005.
- [14] T. Aoki, A. Matsunaga, Y. Ogami, A. Maekawa, S. Mitsushima, K. Ota, H. Nishikawa, J. Power Sources 195 (2010) 2182–2188.
- [15] G.A. Gruver, R.F. Pascoe, H.R. Kunz, J. Electrochem. Soc. 127 (1980) 1219–1224.
- [16] K. Kinoshita, J.T. Lundquist, P. Stonehart, J. Electroanal. Chem. 48 (1973) 157–166.
- [17] K. Yasuda, A. Taniguchi, T. Akita, T. Ioroi, Z. Siroma, Phys. Chem. Chem. Phys. 8 (2006) 746–752.
- [18] E. Antolini, E.R. Gonzalez, Solid State Ionics 180 (2009) 746–763.
- [19] S.G. Neophytides, K. Murase, S. Zafeirotas, G. Papakonstantinou, F.E. Paloukis, N.V. Krstajic, M.M. Jaksic, J. Phys. Chem. B 110 (2006) 3030–3042.
- [20] S. Meyer, S. Saborowski, B. Schafer, Chem. Phys. Chem. 7 (2006) 572–574.
- [21] H.A. Gasteiger, Electrochemistry 75 (2007) 103.
- [22] F.T. Wagner, S.G. Yan, P.T. Yu, Catalyst and Catalyst-support Durability, in: Handbook of Fuel Cells: Fundamentals, Technology and Applications, Advances in Electrocatalysis, Materials, Diagnostics and Durability, vol. 5, Wiley, Chichester, UK, 2009, p. 250.
- [23] Y.-J. Wang, D.P. Wilkinson, J. Zhang, Chem. Rev. 111 (2011) 7625–7651.
- [24] D. Morris, Y. Dou, J. Rebane, C.E.J. Mitchell, R.G. Egdell, D.S.L. Law, A. Vittadini, M. Casarin, Phys. Rev. B 61 (2000) 13445–13457.
- [25] J. Arbiol, J. Cerda, G. Dezanneau, A. Cirera, F. Peiro, A. Cornet, J.R. Morante, J. Appl. Phys. 92 (2002) 853–861.
- [26] A. Bernasik, M. Radecka, M. Rekas, M. Sloma, Appl. Surf. Sci. 65 (1993) 240–245.
- [27] K.-W. Park, K.-S. Seol, Electrochem. Commun. 9 (2007) 2256–2260.
- [28] A. Ruiz, G. Dezanneau, J. Arbiol, A. Cornet, J. Morante, Chem. Mater. 16 (2004) 862–871.
- [29] <http://www.chemicool.com/elements/palladium.html>.
- [30] A.S. Fialkov, Russ. J. Electrochem. 36 (2000) 3845–3866.
- [31] J. Escard, C. Leclère, J.P. Contour, J. Catal. 29 (1973) 31–39.
- [32] G. Brauchotte, G. Cizeron, J. Mater. Sci. 24 (1989) 3123–3136.
- [33] J.R. Martinelli, S.T. dos Reis, Electrical Characterization of Zirconia–Niobium and Zirconia–Titanium Composites, in: Ceramic Transactions, Advances in Ceramic–Matrix Composites, vol. 38, 1993, p. 521.
- [34] G. Hohenberger, G. Tomandl, R. Ebert, T. Taube, J. Am. Ceram. Soc. 74 (1991) 2067–2072.
- [35] J.R. Martinelli, F.F. Sene, Ceram. Int. 26 (2000) 325–335.
- [36] J. Mitra, A.K. Raychaudhuri, Phys. Rev. B 68 (2003) 134428.
- [37] S. Bhattacharyya, S.J. Henley, D. Lock, N.P. Blanchard, S.R.P. Silva, Appl. Phys. Lett. 89 (2006) 022113.
- [38] A. Rochefort, P. Avouris, J. Phys. Chem. A 104 (2000) 9807–9811.
- [39] J. Kieffer, J.B. Wagner Jr., J. Electrochem. Soc. 135 (1988) 198–205.
- [40] B.L. García, R. Fuentes, J.W. Weidner, Electrochem. Solid-State Lett. 10 (2009) B108–B110.
- [41] H. Chhina, D. Susac, S. Campbell, O. Kesler, Electrochem. Solid-State Lett. 12 (2009) B97–B100.
- [42] S. Padmanabhan, S. Pillai, J. Colreavy, S. Balakrishnan, T. Perova, Y. Gun'ko, Y.S. Hinder, J. Kelly, Chem. Mater. 19 (2007) 4474–4481.
- [43] A.L. Patterson, Phys. Rev. 56 (1939) 978–982.
- [44] C.-M. Chen, M. Chen, H.-W. Yu, S.-C. Lu, C.-F. Chen, Jpn. J. Appl. Phys. 47 (2008) 2324–2329.
- [45] Y.-Y. Chu, Z.-B. Wang, D.-M. Gu, G.-P. Yin, J. Power Sources 195 (2010) 1799–1804.
- [46] E. Antolini, F. Cardellini, J. Alloys Compd. 315 (2001) 118–122.
- [47] Y.-H. Qin, Y. Jiang, D.-F. Niu, X.-S. Zhang, X.-G. Zhou, L. Niu, W.-K. Yuan, J. Power Sources 215 (2012) 130–134.
- [48] H. Li, G. Sun, N. Li, S. Sun, D. Su, Q.J. Xin, Phys. Chem. C 111 (2007) 5605–5617.
- [49] R. Larsen, R.I. Masel, Electrochem. Solid-State Lett. 7 (2004) A148–A150.
- [50] R.S. Jayashree, J.S. Spendlow, J. Yeom, C. Rastogi, M.A. Shannon, P.J.A. Kenis, Electrochim. Acta 50 (2005) 4674–4682.
- [51] A. Cuesta, A. Couto, A. Rincon, M.C. Perez, A. Lopez-Cudero, C. Gutierrez, J. Electroanal. Chem. 586 (2006) 184–195.
- [52] M. Lukaszewski, K. Kusmierczyk, J. Kotowski, H. Siwek, A. Czerwinski, J. Solid State Electrochem. 7 (2003) 69–76.
- [53] J. Schmidt, H.A. Gasteiger, G.D. Stäb, P.M. Urban, D.M. Kolb, R.J. Behm, J. Electrochem. Soc. 145 (1998) 2354–2358.
- [54] A. Tegou, S. Papadimitriou, I. Mintsouli, S. Argyrakov, E. Valova, G. Kokkinidis, S. Sotiropoulos, Catal. Today 170 (2011) 126–133.
- [55] P. Mani, R. Srivastava, P. Strasser, J. Power Sources 197 (2011) 666–673.
- [56] A. Marcu, G. Toth, R. Srivastava, P. Strasser, J. Power Sources 208 (2012) 288–295.
- [57] H.I. Karan, K. Sasaki, K. Kuttijyel, C.A. Farberow, M. Mavrikakis, R.R. Adzic, ACS Catal. 2 (2012) 817–824.
- [58] C. Koenigsmann, E. Sutter, T.A. Chiesa, R.R. Adzic, S.S. Wong, Nano Lett. 12 (2012) 2013–2020.
- [59] A.J. Bard, L.R. Faulkner, Electrochemical Methods: Fundamentals and Applications, second ed., John Wiley & Sons, New York, NY, 2001, 196.
- [60] E. Higuchi, H. Uchida, M. Watanabe, J. Electroanal. Chem. 583 (2005) 69–76.
- [61] D.R. Lawson, L.D. Whiteley, C.R. Martin, M.N. Szentimay, J.I. Song, J. Electrochem. Soc. 135 (1988) 2247–2253.
- [62] H.R. Colón-Mercado, B.N. Popov, J. Power Sources 155 (2006) 253–263.
- [63] J. Jiang, B. Yi, J. Electroanal. Chem. 577 (2005) 107–115.
- [64] E. Antolini, Energy Environ. Sci. 2 (2009) 915–931.